



Strain Rate Dependent Nanostructure of Hydrogels with Reversible Hydrophobic Associations During Uniaxial Extension

Journal:	<i>Soft Matter</i>
Manuscript ID	SM-ART-10-2018-002165
Article Type:	Paper
Date Submitted by the Author:	24-Oct-2018
Complete List of Authors:	Wang, Chao; University of Akron, Polymer Engineering Wiener, Clinton; University of Akron, Department of Polymer Engineering Fukuto, Masafumi; Brookhaven National Laboratory, Condensed Matter Physics and Materials Science Department Li, Ruipeng; Cornell University, CHESS Yager, Kevin; Brookhaven National Laboratory, Center for Functional Nanomaterials Weiss, Robert; University of Akron, Department of Polymer Engineering Vogt, Bryan; University of Akron, Polymer Engineering



Strain Rate Dependent Nanostructure of Hydrogels with Reversible Hydrophobic Associations During Uniaxial Extension

Chao Wang,^a Clinton G. Wiener,^a Masafumi Fukuto,^b Ruipeng Li,^b Kevin G. Yager,^c R. A. Weiss,^{*a} Bryan D. Vogt^{*a}

Received 00th January 20xx,
Accepted 00th January 20xx

DOI: 10.1039/x0xx00000x

www.rsc.org/

An energy dissipation mechanism during deformation is required to impart toughness to hydrogels. Here we describe how *in situ* small angle x-ray scattering (SAXS) provides insight into possible energy dissipation mechanisms for a tough hydrogel based on an amphiphilic copolymer where nanoscale associations of the hydrophobic moieties act as effective crosslinks. The mechanical properties of the hydrogels are intimately coupled with the nanostructure that provides reversible crosslinks and evolves during deformation. As the extension rate increases, more mechanical energy is dissipated from rearrangements of the crosslinks. The scattering is consistent with hopping of hydrophobes between the nanoscale aggregates as the primary rearrangement mechanism. This rearrangement changes the network conformation that leads to non-affine deformation, where the change in the nanostructure dimension from SAXS is less than 15% of the total macroscopic strain. These nanostructure changes are rate dependent and correlated with the relaxation time of the hydrogel. At low strain rate (0.15 %/s), no significant change of the nanostructure was observed, whereas at higher strain rates (1.5%/s and 8.4 %/s) significant nanostructure anisotropy occurred during extension. These differences are attributed to the ability for the network chains to rearrange on the time scale of the deformation; when the characteristic time for extension is longer than the average segmental relaxation time, no significant change in nanostructure occurs on uniaxial extension. These results illustrate the importance of strain rate in the mechanical characterization and consideration of relaxation time in the design of tough hydrogels.

Introduction

Hydrogels with reversible (supramolecular) crosslinks have potential application in tissue engineering¹ as well as technologies where self-healing² or shape memory³ properties are desired due to their high toughness and ability to resist catastrophic failure.⁴ During deformation, the reversible crosslinks, such as hydrophobic associations,⁵ ionic bonds,⁶ and/or hydrogen bonding,⁷ will rearrange to dissipate mechanical energy, effectively breaking and re-forming the crosslink. Since the rearrangements of these crosslinks depend on the time scale of the deformation,⁸ the evolution of mechanical properties and

structure of supramolecular hydrogels should be dependent on the strain rate. As the strain rate increases, the network chains connecting two reversible crosslinks will become more extended at a given strain, due to decreased time for relaxation. This extended chain conformation should produce higher forces on the reversible crosslinks. As this stress provides energy to facilitate breaking supramolecular bonds, the strain-rate should relate directly to the crosslink dynamics (dissociation/association). The changes in the nanostructure and mechanical properties of a supramolecular hydrogel should be directly related, but strain rate dependent. Understanding the origin of this strain rate dependency is important for controlling the mechanical performance of tough hydrogels with reversible crosslinks, but direct observations of the deformation rate changes in the microstructure are challenging.

A responsive nanogel based on complementary nonradiative resonance energy transfer has been developed to elucidate the local strain in the hydrogel in real time,⁹ but this approach requires material-specific chemistry and sensitivity is limited by the critical (Förster) radius between donor and acceptor, typically 1–4 nm.¹⁰ *In situ* small angle neutron scattering (SANS) of a supramolecular hydrogel provides a route to determine the

^a Department of Polymer Engineering, University of Akron, Akron, OH 44325, USA.

^b National Synchrotron Light Source II, Brookhaven National Laboratory, Upton, New York 11973, USA.

^c Center for Functional Nanomaterials, Brookhaven National Laboratory, Upton, New York 11973, USA.

Electronic Supplementary Information (ESI) available: Illustration for sector average. 1-dimensional scattering profiles in parallel and perpendicular directions during uniaxial extension. Fitting of 1-dimensional profile with the broad peak model. Macroscopic strains in parallel and perpendicular directions during uniaxial extension. Parameters for the three stretched exponentials fit to the stress relaxation response. Generalized Maxwell Model with residual stress fit to the stress relaxation response. See DOI: 10.1039/x0xx00000x

microstructure change during stress relaxation after deformation, which was found to correlate well with the stress relaxation behavior of the hydrogel.¹¹ However, the time resolution for SANS is limited, so measurements during deformation that could provide insights in the strain rate dependence of the microstructure were not possible. For hybrid (covalent and supramolecular crosslinks) hydrogels, models have been developed to describe the dynamics of the deformation of dual networks^{12, 13} and the rate dependent mechanical properties.¹⁴ Despite the success of these models, detailed understanding of how supramolecular crosslinks evolve during deformation and the relationship of this structure to mechanical properties remains elusive.

Here, we demonstrate *in situ* x-ray scattering during uniaxial extension to elucidate the strain rate dependent microstructure evolution of a supramolecular hydrogel. The hydrogel was based on a random copolymer of 2-(N-ethylperfluorooctane sulfonamido)ethyl acrylate (FOSA, 9.7 mol%) and N,N-dimethylacrylamide (DMA), denoted as DF10, where the aggregates of the hydrophobic FOSA acts as reversible crosslinks. As illustrated pictorially in Figure 1(a), the DF10 hydrogel is known to exhibit a core-shell nanostructure consisting of hydrophobic, glassy FOSA-rich cores (45–46 Å diameter¹¹) surrounded by a water depleted poly(DMA) shell, which are interconnected by hydrated poly(DMA) network chains.^{15, 16} The FOSA-rich nanodomains are reversible crosslinks that provide a mechanism for energy dissipation by release of network chains during deformation and the energy penalty for dispersal of FOSA in water provides driving force to reform the crosslink after the stress is dissipated. The *in-situ* synchrotron x-ray measurements provide insight into the mechanisms at the nanoscale for these reversible crosslinks.

Experimental

Materials

2-(N-ethylperfluorooctane-sulfonamido) ethyl acrylate (FOSA, 95.0%) was purchased from BOC Sciences. The FOSA was purified by dissolution in methanol at 60 °C and subsequent recrystallization at 0°C. N,N-Dimethylacrylamide (DMA, 99.9 %) was purchased from Sigma-Aldrich, dried with calcium hydride (Sigma-Aldrich Chemical Co., reagent grade, 95%) and then purified by distillation under reduced pressure (635 mm Hg) at 60 °C. 2,2'-Azobis(2-methylpropionitrile) (AIBN, ≥98.0%) was purchased from Sigma-Aldrich and recrystallized from methanol. 1,4-dioxane (≥99.0%), N,N'-Methylene bis(acrylamide) (MBAA) was purchased from Sigma-Aldrich and used as received.

The DMA-FOSA copolymer was synthesized by free radical solution polymerization. 10.1 g DMA and 7.50 g FOSA were dissolved in 160 g 1,4-dioxane in a 250 ml round bottom flask and

magnetically stirred at 700 rpm. The solution was sparged with dry nitrogen gas for 1 h using a needle inserted through a rubber septum to remove oxygen. The solution was subsequently heated to 60 °C with an oil bath. 0.0162 g AIBN dissolved in 10.0 g 1,4-dioxane was sparged with dry nitrogen for 5 min. Polymerization was initiated by injecting the AIBN solution into the monomer solution. The solution was purged with dry nitrogen gas for 2 h after the initiator was injected. After 36 h, the reaction was terminated by cooling to room temperature and exposing the solution to ambient air. The product solution was concentrated to 40% of its original volume using a rotary evaporator at 40 °C and 16 kPa. The DMA/FOSA copolymer was recovered by precipitating the concentrated solution in 600 mL of diethyl ether at 0 °C. The precipitate product was then dried under vacuum at 50 °C for 48 h.

The hydrogel samples were prepared by vacuum (~4.0 kPa) compression molding the dry DMA/FOSA copolymer at 160 °C into ~0.50-mm-thick sheets under 4.4×10^5 N for 2 h using a Technical Machine Products 35-ton vacuum molding machine. These copolymer sheets were immersed in excess Type 1 ultrapure water (Milli-Q, Millipore) for at least 7 days at room temperature (~22 °C). The mass of the hydrogel was monitored every 24 h using a Mettler Toledo XS104 Excellence XS Analytical Balance to ensure that the hydrogel reached equilibrium. When the mass changed by < 3 % over 48 h, we defined the hydrogel as being at equilibrium. After swelling, the average thickness of the hydrogel sheet was approximately 0.7 mm.

In-Situ Small Angle X-ray Scattering (SAXS)

The equilibrium swollen hydrogel sheets were cut into tensile bars with gauge length of ≈10.0 mm and gauge width of ≈5.78 mm. The mechanical properties of these tensile bars were measured using the Linkam TST350 tensile stage with the standard quartz windows replaced by 100 μm thick Kapton (DuPont) for X-ray transparency. The hydrogels were uniaxially elongated at 0.15%/s, 1.5%/s and 8.4%/s to 75% strain. These data were reported in terms of the engineering stress, $\sigma = F/A_0$, where F is the force applied to the tensile bar and A_0 is the cross-sectional area of the gauge section, and the engineering strain, $\epsilon = \Delta l/l_0$, where l_0 is the initial gauge length, and Δl is the change of gauge length during elongation. A camera was placed in the hutch during the stretching to determine the macroscopic dimensional change in directions parallel (length) and perpendicular (width) to stretching. The stress relaxation behavior of the hydrogel was determined by stretching at 8.4%/s to 75% strain. The sample was held at this strain and the stress decay at constant strain was subsequently monitored for 1200 s. The microstructure of the hydrogel during elongation and stress relaxation was simultaneously probed by SAXS. The SAXS measurements were carried at the 11-BM CMS beamline at the National Synchrotron

Light Source II (NSLS II) using 13.5 keV X-rays (wavelength, λ , = 0.918 Å) and a Dectris Pilatus 300K detector (pixel size = 0.172 mm \times 0.172 mm) with a sample-to-detector distance of 202 cm. During the stretching, the scattering was collected for 1 s with \approx 0.8 s intervals between measurements. To minimize beam damage, 12 positions approximately 0.2 mm apart were sequentially cycled for the SAXS measurements.

The SAXS data were reduced using the Nika package in Igor Pro 6.37.¹⁷ The background scattering was subtracted from the raw scattering data and the detector mask associated with the beam stop and the gaps between detector pixels was applied. As the scattering becomes anisotropic from the uniaxial elongation, the reduced 2-dimensional data were azimuthally averaged in sectors associated with the parallel (0° azimuthal) or perpendicular (90° azimuthal) direction (width \pm 22°) as shown in Figure S1(a) with respect to the elongation direction to obtain 1-dimensional scattering patterns as a function of the scattering vector, q , (Figure S2). The predominate feature in the scattering data was a correlation peak centered at $q \approx 0.096 \text{ \AA}^{-1}$ before stretching. To interpret the SAXS data during uniaxial extension, an appropriate model must be applied. To avoid overinterpretation of the scattering data, three different models with different assumptions were examined:

Previously, the broad peak model has been applied to provide an empirical fit of the scattering data for analogous hydrogels based on copolymers^{18, 19} and has also been successfully applied to a variety of soft materials²⁰⁻²³ to interpret their small angle scattering. The form of the broad peak model is shown in Equation (1):

$$I(q) = \frac{A}{1 + (|q - q_0|\zeta)^m} + bkg \quad (1)$$

where ζ is a correlation length for inter-nanodomain positional correlations, m is the Lorentzian exponent and q_0 is the peak position, which is related to the interdomain spacing (characteristic distance between scattering heterogeneities) by $D_i = 2\pi/q_0$. A is the Lorentzian amplitude and bkg is the background. Examples of the fits to the scattering profiles are shown in Figure S2. The full width at half maximum (FWHM = $2/\zeta$) of the scattering peak can be interpreted in terms of the distribution of D_i , with the FWHM decreasing for a narrower distribution. This FWHM was independent of ε and $\dot{\varepsilon}$ (FWHM \approx 0.040 \AA^{-1}) for the scattering from the hydrogel. This invariance suggests that the distribution of center-to-center distances about the mean was unchanged by the stretching of the hydrogel.

Recently, the scattering for hydrogel based on a well-defined block copolymer crosslinked by spherical hydrophobic domains

was described by a hard sphere model.²⁴ The hard sphere model²³ is shown in Equation (2):

$$I(q) = n_p V_p^2 (\Delta\rho)^2 P(q) S(q) + bkg \quad (2)$$

where n_p is the number density of the spheres (core-shell nanodomains), V_p is the sphere volume, $\Delta\rho$ is the scattering length density difference between the spheres and water.

This model uses a Percus–Yevick hard-sphere interaction potential to describe the partial structure factor, $S(q)$, of the spherical crosslinks, while the Debye–Bueche model was used for the partial structure factor of the network chains. This later contribution is an empirical model in the same class as the broad peak model. This model also includes the form factor, $P(q)$, for spheres:

$$P(q) = \left\{ \frac{3[\sin(qr) - qr\cos(qr)]}{(qr)^3} \right\}^2 \quad (3)$$

where r is the radius of the nanodomains.

The final model examined is the unified model approach developed by Beaucage²⁵ that can be used to describe a wide variety of correlated systems. The general form for this model is shown in Equation (5):

$$I(q) = \sum_{i=1}^n \frac{(G_i \exp\left(\frac{-q^2 R_{g,i}^2}{3}\right) + B_i (q_i^*)^{-P_i})}{1 + p_i \theta_i(q)} + bkg \quad (5)$$

where n reflects the number of structure levels and $R_{g,i}$ is the radius of gyration of the structural units in each level. Assuming spherical nanodomains, $(R_{g,i})^2 = (3/5)r_i^2$. G_i is related to the contrast, which includes the number concentration of structural units described by $R_{g,i}$, and the square of the number of electrons.²⁵ B_i is correlated to the contrast and characteristic sizes specific to the type of structure.²⁵ P_i is a Porod exponent. p_i is the packing factor that equals to 8 times the ratio of the occupied to the available volume.²⁵

$$q_i^* = \frac{q}{\left\{ \text{erf}\left(\frac{kqR_{g,i}}{\sqrt{6}}\right) \right\}^3} \quad (6)$$

where $k = 1$,²⁵ and

$$\theta_i(q) = 3 \frac{\sin q\zeta - q\zeta \cos q\zeta}{(q\zeta)^3} \quad (7)$$

where ζ is the correlation length correlated to the average center-to-center distance between the structure units.

Additional insights to the nanostructure anisotropy during uniaxial deformation were gleaned from examination of the azimuthal dependence of the scattered intensity. The 2-dimensional SAXS patterns were azimuthally averaged in sectors every 5° (width $\pm 2.5^\circ$) from 0° to 180° , Figure S1(b). The correlation peak centered at $q \approx 0.096 \text{ \AA}^{-1}$ before stretching in each resulting 1-dimensional pattern was fit to the broad peak model, Equation (1). Both the intensity of the peak from the Lorentzian amplitude A (i.e. the background subtracted intensity of the correlation peak) and the peak position (q_0) were examined as a function of azimuthal angle. In order to account for the effect of the sample thickness on the Lorentzian amplitude A , the fit values for A were multiplied by the factor (T_0/T_ϵ) , where T_0 is the sample thickness before stretching, and T_ϵ is the sample thickness at strain ϵ . Also, each A in Figure S7 was shown as the average of 5 neighboring points to reduce the uncertainty that originated from the azimuthal average over a small angle (5°).

Results and discussion

Small angle scattering and the mechanical properties of the DF10 hydrogel during uniaxial extension were measured simultaneously. The hydrogel was stretched to a strain (ϵ) of 75% at three different strain rates: $\dot{\epsilon} = 0.15\%/s$, $1.5\%/s$ and $8.4\%/s$. As the strain rate increased, the area beneath the stress-strain curve increased, Figure 1(b). That result suggests additional mechanical energy was dissipated at higher strain rates due to additional rupturing or deformation of the physical crosslinks. The macroscopic response to the extension was recorded with cameras to independently monitor the strain and width of the specimen. Within the linear-elastic region, a rate-dependent Poisson's ratio was observed (Figure S3). The apparent Poisson's ratio was approximately 0.5 for the slower stretching rates ($0.15\%/s$ and $1.5\%/s$), but decreased to ≈ 0.4 at for $\dot{\epsilon} = 8.4\%/s$. This behavior, within the linear-elastic region, is similar to that for elastomers. At slow elongation rates, the network chains can rearrange/relax to accommodate the deformation. At faster elongation rates, however, the response to deformation is likely impacted by the deformation of the glassy FOSA domains,¹¹ which have a Poisson's ratio $\approx 1/3$ that decreases the apparent Poisson's ratio for the hydrogel. These macroscopic scale differences in the response to deformation rate during uniaxial elongation should lead to different nanoscale changes as well.

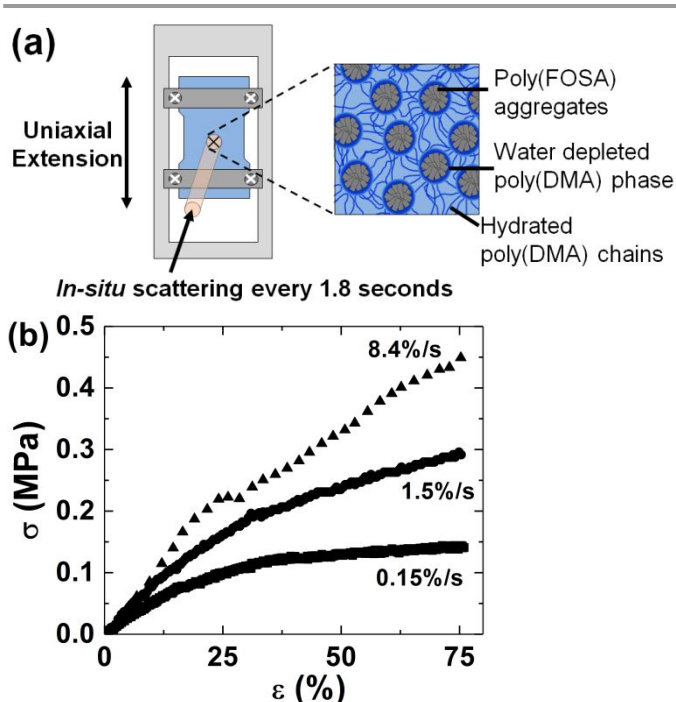


Figure 1. (a) Schematic illustration of the nanostructure of DF10 hydrogels and the *in situ* SAXS measurements during uniaxial extension. Schematic is not to scale. (b) Stress-strain (σ - ϵ) curves as a function of strain rates on uniaxial extension to 75% strain obtained during the SAXS measurements.

Figure 2 illustrates the 2D scattering patterns obtained from *in situ* SAXS. For the lowest rate examined ($0.15\%/s$), the scattering pattern appears almost unchanged (Figure 2a) after stretching to 75% strain. There is a decrease in the scattered intensity associated with the correlation ring due to thinning of the sample during the stretch. At $1.5\%/s$ (Figure 2b), the scattering ring becomes slightly anisotropic with the maximum intensity moving to a slightly lower q_x and larger q_y . This change becomes more pronounced at $8.4\%/s$ (Figure 2c) with an ellipsoid scattering pattern visually resolved after stretching to 75% strain. The nanostructure change on uniaxial elongation was quantified using azimuthal sector averages of the 2D scattering patterns to obtain 1-dimensional profiles that are primarily parallel (azimuthal angle $\alpha = 0^\circ \pm 22^\circ$) and primarily perpendicular ($\alpha = 90^\circ \pm 22^\circ$) to the stretching direction, Figure S1(a). The average change in the interdomain spacing (D_i , center-to-center distance between core-shell nanodomains) during extension was determined from the correlation peak centered at $q \approx 0.096 \text{ \AA}^{-1}$ before stretching, Figure S4. The changes in the interdomain spacing (D_i) that are parallel ($D_{//}$) and perpendicular (D_{\perp}) to the stretching direction were determined by fitting the sector averaged scattering profiles to appropriate models.

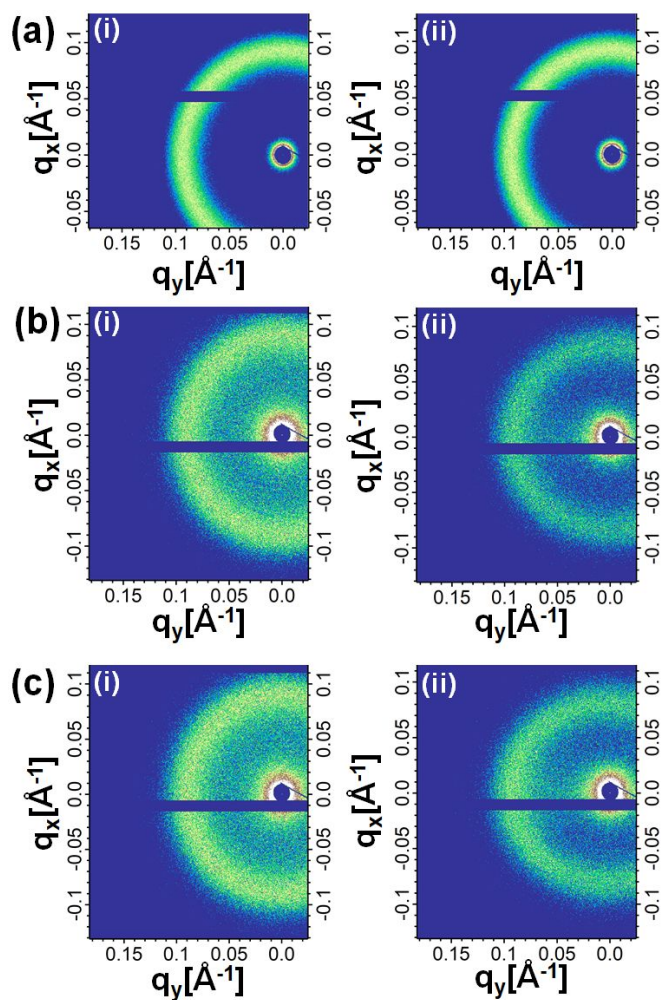


Figure 2. SAXS scattering patterns at (i) 0% strain and (ii) 75% strain during 1-D extension at strain rates of (a) 0.15%/s (b) 1.5%/s and (c) 8.4%/s.

The sector averaged data can be well fit by all three models; Broad peak (BP), hard sphere (HS)²³ and the unified generalized model developed by Beaucage (BC);²⁵ as shown in Figure S5. Unsurprisingly as it has been used to fit similar hydrogels,^{18, 19} the BP model fits the peak in the scattering profile well (Figure S5a). However, the empirical nature of the BP model does somewhat limit the physical insights, but the fit provides the average center-to-center distance (D_i) between the FOSA nanodomains. The hard sphere model, which provides additional information about the size of the FOSA nanodomains, does not fit the scattering data well at high q as shown in Figure S5b. The unified model fits the scattering data well (Figure S5c) and provides information about the domain spacing and the size of the FOSA nanodomains. As shown in Figure 3, the D_i change during uniaxial extension at $\dot{\epsilon} = 8.4\%/s$ is similar between the three models, but there is a quantitative difference in the initial spacing and extent of change. When the hydrogel was stretched to $\epsilon = 75\%$, $D_{//}$ increased 21% and D_{\perp} increased 1.7% from the HS fits. The BC model suggests

that $D_{//}$ increased 9.4% and D_{\perp} decreased 4.0%, which is similar to the BP model where that $D_{//}$ increased 10.0% and D_{\perp} decreased 2.4%. The qualitative difference in the effect of stretching on D_{\perp} may be related to the poor fit of the data to the HS model at high q , although the overall change in dimensions is very small in all cases. A similar behavior in terms of the fit at high q for the HS model has been reported previously for hydrogels from well-defined block copolymers as well.²⁴ The size of the FOSA domains is found to increase parallel to the deformation and decrease perpendicular when the data was fit with the HS model, but counter to the effect on size obtained from the BC model, Figure S6. As both the HS and BC models have been shown to quantitatively describe the structures of similarly nanostructured soft materials, we cannot determine information about how the size of the FOSA domains change during deformation and will focus on the changes in D_i . As shown in Figure 3, there is reasonable agreement in the qualitative effect of stretching on D_i for the 3 models examined.

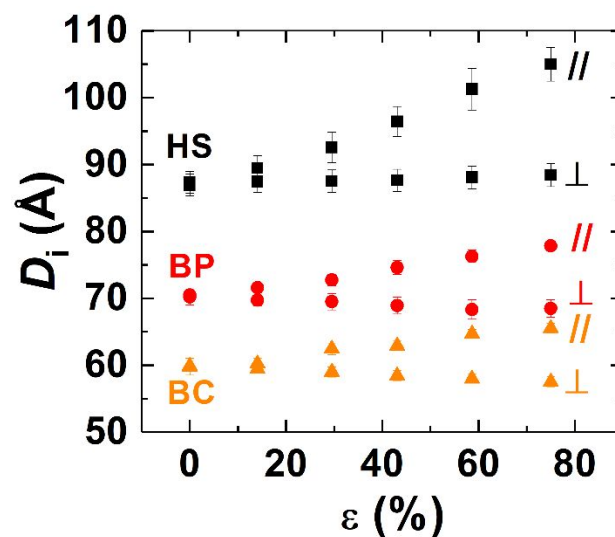


Figure 3. The interdomain spacings (D_i) for the DF10 hydrogel parallel ($//$) and perpendicular (\perp) to the stretching direction at a strain rate of 8.4%/s estimated by the broad peak model (BP, ●), hard sphere model (HS, ■) and unified model of Beaucage (BC, ▲).

Figure 4 shows the influence of strain rate on $D_{//}$ and D_{\perp} as determined from the BP model, which provided intermediate values for D_i (Figure 3). At low strain rate ($\dot{\epsilon}$) (Figure 4a), the changes in D_i were small with $<0.5 \text{ \AA}$ change during the uniaxial extension to $\epsilon = 75\%$. For $\dot{\epsilon} = 1.5\%/s$ (Figure 4b), D_i increased nearly linearly with strain with a 4.5 \AA increase in $D_{//}$ at $\epsilon = 75\%$. Despite the yielding behavior for $\dot{\epsilon} = 8.4\%/s$, $D_{//}$ and D_{\perp} changed almost linearly with increasing strain (Figure 4c) and $D_{//}$ increased 7.3 \AA at $\epsilon = 75\%$. This linear relationship was qualitatively consistent with the macroscopic dimension changes during uniaxial extension (Figure S3). The increasing anisotropy in D_i at higher strain rates was consistent with the increasing amplitude of the peak that emerges in the azimuthal angle dependent

Lorentzian amplitude (A), Figure S7. However, quantitative changes in D_i were small compared to the changes in macroscopic dimensions. For example, when the hydrogel was stretched to $\varepsilon = 75\%$, $D_{//}$ only increased by 0.30%, 6.4% and 10% for $\dot{\varepsilon} = 0.15\%/s$, 1.5%/s and 8.4%/s, respectively. Similarly, the macroscopic width of the hydrogel perpendicular to the extension decreased by 16–23%, while D_{\perp} decreased by only 2.3%, 2.1% and 2.4% for $\dot{\varepsilon} = 0.15\%/s$, 1.5%/s and 8.4%/s, respectively.

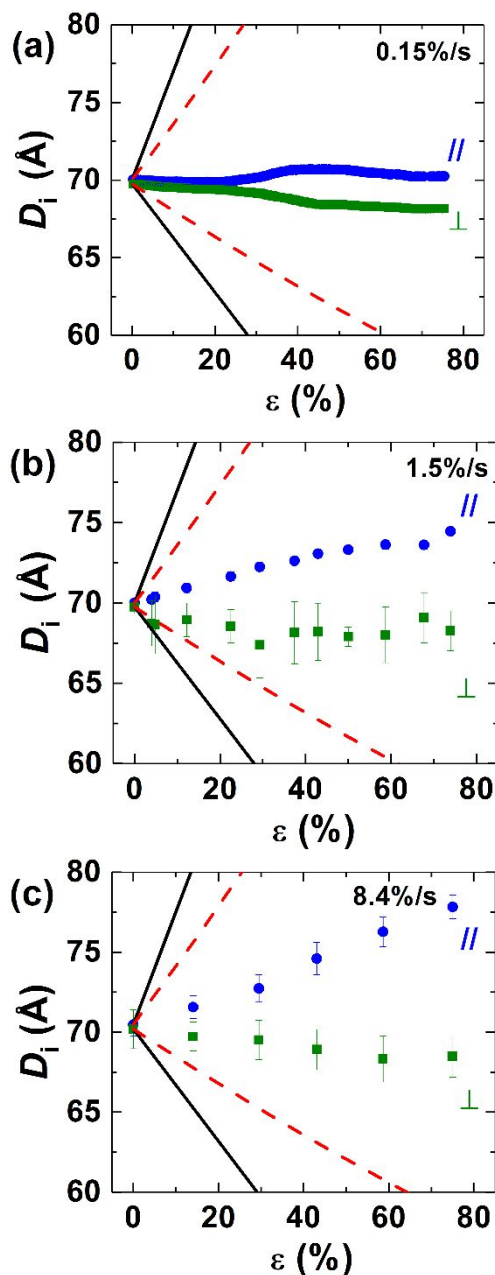


Figure 4. The interdomain spacings (D_i) for the DF10 hydrogel parallel ($//$) and perpendicular (\perp) to the stretching direction at strain rates of (a) 0.15%/s (b) 1.5%/s and (c) 8.4%/s. The error bars correspond to the uncertainty in the fit. In some cases, error bars are smaller than the size of the symbol. The black solid lines show the prediction of the affine network

model, and the red dashed lines show the prediction from the phantom network model with a functionality of 4.

If the topology of the crosslinks were fixed, these large differences in the dimensional changes at different length scales would cause a large decrease in the mass density²⁶ of the hydrogel and lead to void formation or increasing water absorption. However, no change in the mass of the DF10 hydrogel and no void formation were observed. Moreover, a previous study on the DF10 hydrogel demonstrated that when stretched at approximately $\dot{\varepsilon} = 33\%/s$ to $\varepsilon = 150\%$, the volume fraction of FOSA nanodomains increased 6.22%.¹¹ In this study where the maximum strain and strain rate were smaller, a smaller increase in the volume fraction of nanodomains was expected. Nevertheless, an increase in the volume fraction of nanodomains is not consistent with void formation or water mass increase, both of which would decrease the nanodomain volume fraction. The black and red solid lines in Figure 4 are the affine and phantom network model predictions for a covalently crosslinked hydrogel with a functionality of 4. The changes in $D_{//}$ and D_{\perp} shown in Figure 4 deviate considerably from the predictions of affine or phantom network models with covalent crosslinks²⁶. In general, the behavior of a real network is expected to fall between those two model predictions. There are approximately 70 FOSA groups in each nanodomain, but only a fraction of these are expected to form effective crosslinks due to the random nature of the copolymerization. This leads to some uncertainty in the exact functionality of the nanodomains, but the actual changes in D_i are always less than either model, irrespective of the functionality selected. The deviation between the phantom chain model and actual dimensions increases as the functionality increases (Figure S8). The large difference in the changes in the microscopic dimensions for the DF10 hydrogel compared with the affine and phantom network models is a consequence of the reversible nature of the supramolecular crosslinks that allows the nanostructure to rearrange during deformation.

The differences between the macro- and micro-deformations of the DF10 hydrogel can be more clearly understood by considering the schematic microstructures shown in Figure 5. Initially the network microstructure is isotropic, Figure 5(i). During an affine deformation of a network with fixed crosslinks, $D_{//}$ increases and D_{\perp} decreases proportional to the macroscopic deformation, Figure 5(ii). For the uniaxial extension of a hydrogel with reversible crosslinks such as DF10, Figure 5(iii), the “hopping” of FOSA groups changes the connections between nanodomains and alters the network configuration to stretch the network chains and align the nanodomains (i.e., the crosslink junctions) in the parallel direction. The FOSA-hopping (i.e., rearrangement of the network chains) relax the stresses in the network chains, which results in a much smaller increase of $D_{//}$ and decrease of D_{\perp} than would be expected if the crosslinks were fixed, i.e., the deformation was affine. As this hopping mechanism only involves

the transfer of a small number of FOSA groups from the approximately 70 FOSA groups that comprises the nanodomain, the scattering would be relatively insensitive to these events, which is consistent with the *in-situ* SAXS measurements. As SAXS averages the structure, we cannot rule out rare events where the FOSA nanodomains break and then reform, but this would be unlikely given the large volume probed by the beam relative to the correlation distance and the significant difference between the nanoscale dimension changes and those macroscopically during extension. Similarly, rearrangements on the time scale of the measurements (~ 1 s) would not be resolved, but this time scale is likely too short for cooperative re-arrangement events that involve many FOSA groups. Thus, the FOSA jumping mechanism appears to be most probable based on the *in situ* SAXS data.

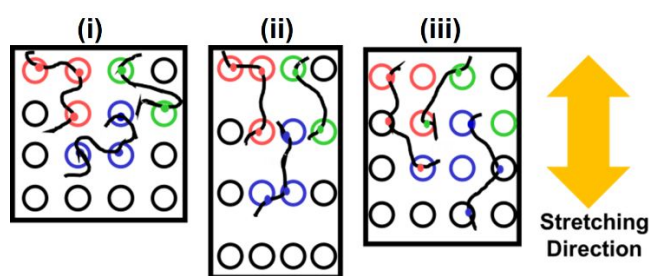


Figure 5. (i) Schematic of an undeformed isotropic network of a supramolecular hydrogel focusing on the behavior of 3 chains (black lines) and 8 FOSA groups (red, green and blue circles). The larger circles represent supramolecular nanodomains (not drawn to scale). The color of the nanodomain corresponds to the color of the FOSA groups occupying it prior to deformation (black nanodomains do not originally contain any of the 8 selected FOSA groups). (ii) Affine deformation of a covalently crosslinked hydrogel (D_{\parallel} increases and D_{\perp} decreases during stretching proportional to the macroscopic changes). (iii) Deformation of the DF10 hydrogel with reversible crosslinks hydrophobic (FOSA) crosslinks. In this case, network chains can rearrange by "hopping" of FOSA groups from one nanodomain to another. As a result of the network rearrangements, the changes of D_{\parallel} and D_{\perp} are less than for a covalent network. Note that it was assumed that the volume of the hydrogel did not change with deformation, Poisson ratio = 0.5 (i.e., the areas of the black boxes in (i), (ii) and (iii) are the same).

The FOSA jumping mechanism, which is proposed to explain the large differences in the macro- and micro-deformations, involves the rearrangements of the effective network chains and segmental relaxation. These dynamic processes can be assessed through the stress relaxation of the hydrogel to further test the proposed FOSA jumping mechanism. The stress relaxation behavior of DF10 stretched to 75% strain at 8.4%/s is shown in Figure 6(a). For many polymers²⁷⁻²⁹, the relaxation behavior can be described by a stretched exponential, but the stress relaxation of DF10 cannot be fit with a single stretched exponential. Thus, a combination of two stretched exponentials, Equation (8), similar to what others have used for stress relaxation of reversible networks,^{28, 30} was used to fit the data in Figure 6(a),

$$\frac{\sigma(t)}{\sigma_0} = A_1 e^{-\left(\frac{t}{\lambda_1}\right)^{\beta_1}} + A_2 e^{-\left(\frac{t}{\lambda_2}\right)^{\beta_2}} \quad (8)$$

where $\sigma(t)/\sigma_0$ is the normalized stress at time t , λ_1 and λ_2 are characteristic average relaxation times, β_1 and β_2 describe the relaxation time distribution and A_1 and A_2 represents the fractional contribution of first and second stretched exponentials to the relaxation behavior respectively. The fit is shown by the solid curve in Figure 6(a), and the fitting parameters are summarized in Table 1. The inclusion of a long relaxation time is consistent with Generalized Maxwell model³¹ fits using 3 – 5 Maxwell elements, which indicated that some very long relaxation time processes were necessary to fit the stress relaxation data, Figure S9.

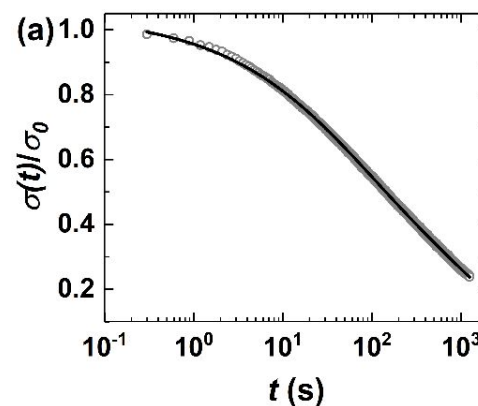
Using the values obtained from the two stretched exponential fit, the probability density of the relaxation time (τ) for each stretched exponential was calculated from Equation (9)³²

$$P_i(s_i, \beta_i) = \frac{1}{\pi} \int_0^{\infty} e^{-u^{\beta_i} \cos\left(\frac{\pi\beta_i}{2}\right)} \cos\left[s_i u - u^{\beta_i} \sin\left(\frac{\pi\beta_i}{2}\right)\right] du \quad (9)$$

where $s_i = \lambda_i/\tau$ and $i = 1$ or 2. The relaxation time distribution is then:

$$H(\tau) = A_1 P_1 + A_2 P_2. \quad (10)$$

Figure 6(c) shows the relaxation time probabilities for the two processes centered at 227 s and 1.14×10^4 s, indicating two groups of relaxation times (short and long) for the DF10 hydrogel based on the stress relaxation experiment.



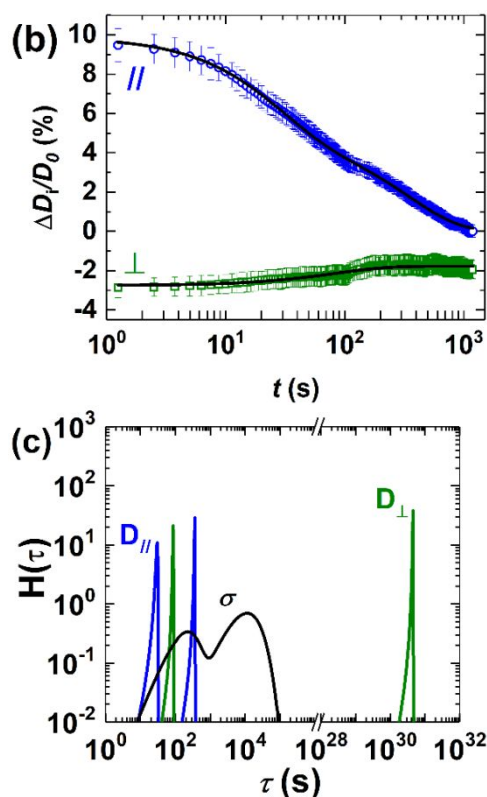


Figure 6. (a) Stress relaxation response for the DF10 hydrogel following a step strain of 75%. The solid line is the fit to two stretched exponentials, Equation (8). (b) The percentage change of D_i parallel ($//$) and perpendicular (\perp) to the stretching direction comparing to the unstretched state ($\Delta D_i/D_0$) during the stress relaxation process in (a). The solid line is the fit to two stretched exponentials, Equation (8). (c) The relaxation time distribution $H(\tau)$ obtained from the stress decay in (a) (black curve) and the interdomain spacing decay in (b) in the parallel (blue curve) and perpendicular (green curve) directions for the DF10 hydrogel.

Fast and a slow relaxation processes in physical hydrogels with ionic crosslinks have previously been reported, where the fast process was attributed to the rupture of physical bonds by the elastic contraction from the network chain, and the slow process was related to the reformation of physical bonds that led to effectively “permanent” physical crosslinks within the time period of the measurement.^{6, 33} However, no quantitative analysis on the structural relaxation of the hydrogel was provided to support these hypotheses. For the hydrophobically modified hydrogels

examined here, the *in-situ* SAXS stretching data (Figure 4) do not support a separation of time scales for the breaking and reformation of the physical bonds.

The temporal change of $D_{//}$ and D_{\perp} (determined from the BP model) for the DF10 hydrogel during the stress relaxation experiment, Figure 6(b), were also fit with two stretched exponentials. The behaviors of the structural and stress relaxation are qualitatively similar, although the distribution of the structural relaxation times is significantly narrower. As shown by the blue curve in Figure 6(c), the slower average relaxation time from the $D_{//}$ is similar to the fast relaxation process probed from the stress decay. This suggests that the fast structural relaxation process in the DF10 hydrogel originated from the segmental relaxation of the network chains, while the slower one is likely associated with the FOSA hopping. In contrast, the green curve for the behavior of D_{\perp} indicates a fast relaxation process similar to the average time for the fast stress relaxation, but the slow relaxation process for D_{\perp} is orders of magnitude slower than that for the stress relaxation. The faster process is attributed again to the segmental relaxation. Segmental relaxation dynamics of polymers has been shown to be enhanced by deformation;³⁴ due to Poisson’s ratio, the deformation for D_{\perp} is less, so the relaxation time is slower. The slower relaxation process for D_{\perp} is presumably due to FOSA hopping. This later process is responsible for the very slow recovery of D_{\perp} to its original value during stress relaxation and why full recovery was not achieved in the time frame of these experiments. Thus, we conclude that the fast relaxation is likely Rouse-like motions in the network chains, while the slow process is FOSA-hopping. These time scales are directional due to differences in the applied forces on the chains between the parallel and perpendicular direction of the elongation. This attribution of the Rouse-like motions for the fast relaxation is probably also the case in Refs [6, 33] where the physical crosslinks are ionic as it is unclear why the time scale for dissociation and reformation would be sufficiently separated to be resolved as different relaxation processes.

Table 1. Fit parameters calculated from Equation (8) and (11) for the data in Figure 6(a) and 6(b).

Model	Data	A_1	λ_1 (s)	β_1	A_2	λ_2 (s)	β_2	R	% residual
Eqn (8)	Stress	0.345	35.1	0.496	0.655	1.09×10^3	0.435	N/A	
	$D_{//}$	5.08	27.0	0.97	4.81	347	1.00		
	D_{\perp}	0.982	83.1	1.00	1.78	4.31×10^{30}	1.00		
Eqn (11)	Stress	0.931	168	0.391	N/A			0.140	14.0
	D_{\perp}	0.909	87.6	1.00				1.79	61.8



Soft Matter

ARTICLE

As the nanostructure of the DF10 hydrogel is originally isotropic, the directional structural recovery indicates that the deformation during uniaxial elongation leads to relaxation processes that are dependent on the details of the chain conformation. This leads to the question of the origins of these differences. Whereas, $D_{//}$ fully recovered to its undeformed value during the stress relaxation experiment, D_{\perp} and the stress did not, Figure 6(b). This suggests that the changes in the nanostructure perpendicular to the applied strain are responsible for the long lived finite stress after 1200 s. As we attribute the slower relaxation times to the FOSA hopping, this suggests that the FOSA groups can rearrange readily in $D_{//}$ and not in D_{\perp} . The FOSA hopping process can be promoted by stresses in the network chains breaking FOSA–FOSA hydrophobic bonds. For $D_{//}$, a large tensile stress is being applied, which should promote the FOSA hopping. Conversely, the network chains are compressed in D_{\perp} , thus the FOSA hopping is not promoted. As the DF10 hydrogels are stable materials, the FOSA hopping in the absence of an applied load must be relatively rare, which is consistent with the very slow relaxation of D_{\perp} . Note that the pullout of a FOSA group from the interior of a nanodomain involves breaking the supramolecular bond and diffusion of the FOSA group through a sea of other hydrophobic interactions. As a result, the process of removing an interior FOSA group from a nanodomain may involve many “hops” as the FOSA group forms new hydrophobic bonds with other FOSA groups within the nanodomain. That process will be inherently much slower than pulling out a FOSA group from the surface of the nanodomain, producing a broad distribution of longer relaxation times due to FOSA hopping.

The chain forces required for the occurrence of the rearrangement events in the DF10 hydrogel can be estimated by considering the free energy difference between well-separated hydrophobic segments solvated in water and the cluster (nanodomain) of hydrophobic segments with smaller solvated surface area than separated segments.³⁵ For the DF10 hydrogel, the work needed to pull one FOSA unit from the nanodomain is determined by the work needed to form a cavity in the FOSA nanodomain with the size of a FOSA unit (28.3 Å²),³⁶ the additional solvation free energy from the increased surface area, and the energy needed to disrupt the hydrogen-bonded network of water.³⁷ However, the multifunctional nature of physical crosslinks based on FOSA nanodomains and the probability for poly(DMA) chains to form loops¹⁹ leads to significantly more complexity to provide understanding of the mechanism from a

theoretical perspective. However, ionomers may represent a reasonable analog for these hydrogels where the ionic clusters are highly associative like FOSA for the DF10 hydrogels. Colby and coworkers proposed a reversible gelation model to predict the linear viscoelastic (LVE) behavior of a non-entangled, randomly sulfonated polystyrene, where the relaxation of the polymer network relies on the lifetime of ionic crosslinks (“stickers”).³⁸ To test this model, a wide frequency window is required; for ionomers, time temperature superposition (TTS) has been used,³⁸ but for DF10 increasing temperature decreases the hydration to decrease the dynamics of the DMA,¹⁹ while the FOSA domains soften with increasing temperature. This leads to challenges with TTS, so additional work is required to determine if the LVE behavior of these hydrogels is indeed described by this reversible gelation model.

Note that since the stress and D_{\perp} did not completely relax, the longer relaxation times shown in Figure 6(c) are most likely underestimated. To better account for the permanent deformation of D_{\perp} and/or the residual stress, the decay of stress and D_{\perp} in Figure 6(a) and 6(b) were fit with a modified stretched exponential, Equation (11).

$$\frac{\sigma(t)}{\sigma_0} = A_1 e^{-\left(\frac{t}{\lambda_1}\right)^{\beta_1}} + R \quad (11)$$

Here, only a single stretched exponential was used, and a new parameter, R , was added to the model to account for the permanent deformation/residual stress. The fit is shown by the solid line in Figure S10 and the fit parameters are summarized in Table 1. Comparing to the stress, D_{\perp} has larger residual after 1200 s, which suggests that there is permanent deformation in the direction perpendicular to stretching even after the stress in the network is relaxed.

The relaxation time distribution measured from the stress relaxation behavior also helps explain the microstructure changes observed from the uniaxial stretching experiments, Figure 2 and Figure 4. One can define a characteristic time associated with the deformation, $\lambda \equiv (1/\dot{\epsilon})$. Thus, for the slowest stretching experiment, $\dot{\epsilon} = 0.15\%/s$, the segmental relaxation times are mostly faster than $\lambda = 667$ s, and the network chains are able to relax during the sample deformation. As a result, the changes of $D_{//}$ and D_{\perp} were small. As $\dot{\epsilon}$ increases to 1.5 %/s ($\lambda = 67$ s) and 8.4 %/s ($\lambda = 6.7$ s), less segmental relaxation occurs during the

deformation and larger changes in the nanodomain separation occur. These differences in the ability for the crosslinks to rearrange also corresponds with the deviation in the macroscopic Poisson's ratio from 0.5 expected for gels and observed when the material can rearrange readily at low strain rates (Figure S3) to nearly 0.4 at the fastest rate examined where the crosslinks cannot relax as fast as the material is being strained.

Conclusions

In summary, we have demonstrated with *in-situ* SAXS that the nanostructure during deformation is strain rate dependent. The nanostructure of the DF10 hydrogel can be related to the network conformation and we attribute the differences in the change in spacing between the crosslinks and the macroscopic deformation of the hydrogel to rearrangements of the effective crosslinks through the hopping of hydrophobic groups between nanodomains. The change in the spacing between the effective crosslinks (nanodomains) during deformation increases as the strain rate increases. This effect can be rationalized by the relaxation of the network. At the slowest rate examined (0.15%/s), there was very little change in the nanostructure where the characteristic time of the deformation ($1/\dot{\epsilon}$) was longer than the segmental relaxation. Conversely, at the fastest rate (8.4%/s), the characteristic time was shorter than the segmental relaxation and a significantly greater change was observed in the nanostructure during uniaxial extension. This work provides insight to the molecular origin of the strain rate dependency of physically crosslinked hydrogels and may provide insights into how to consider relaxation processes in the design of tough supramolecular hydrogels.

Conflicts of interest

There are no conflicts to declare.

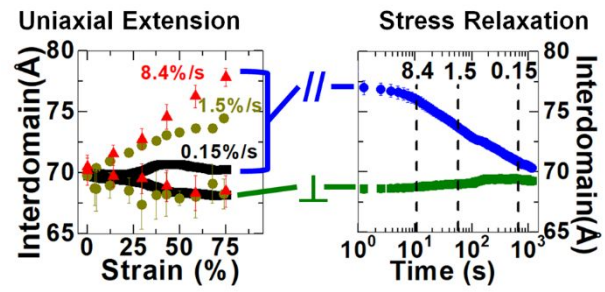
Acknowledgements

This work was financially supported by the Chemical, Bioengineering, Environmental and Transport Systems (CBET) Division in the Directorate for Engineering of the National Science Foundation, grant CBET-1606685. The research used the Complex Materials Scattering (CMS/11-BM) beamline, operated by the National Synchrotron Light Source II and the Center for Functional Nanomaterials, which are U.S. Department of Energy (DOE) Office of Science User Facilities operated for the DOE Office of Science by Brookhaven National Laboratory under Contract No. DE-SC0012704. We thank Xuhui Xia, Yanfeng Xia, Zhiyang Zhao, Fang Peng and Pablo I. Sepulveda-Medina for their help with measurements.

References

1. M. J. Webber, E. A. Appel, E. Meijer and R. Langer, *Nat. Mater.*, 2016, **15**, 13.
2. H. Zhang, H. Xia and Y. Zhao, *ACS Macro Lett.*, 2012, **1**, 1233-1236.
3. Y. Osada and A. Matsuda, *Nature*, 1995, **376**, 219.
4. J.-Y. Sun, X. Zhao, W. R. Illeperuma, O. Chaudhuri, K. H. Oh, D. J. Mooney, J. J. Vlassak and Z. Suo, *Nature*, 2012, **489**, 133.
5. J. Hao and R. Weiss, *Macromolecules*, 2011, **44**, 9390-9398.
6. F. Luo, T. L. Sun, T. Nakajima, T. Kurokawa, Y. Zhao, K. Sato, A. B. Ihsan, X. Li, H. Guo and J. P. Gong, *Adv. Mater.*, 2015, **27**, 2722-2727.
7. D. Myung, D. Waters, M. Wiseman, P. E. Duhamel, J. Noolandi, C. N. Ta and C. W. Frank, *Polym. Adv. Technol.*, 2008, **19**, 647-657.
8. W. Kauzmann and H. Eyring, *J. Am. Chem. Soc.*, 1940, **62**, 3113-3125.
9. M. Zhu, D. Lu, S. Wu, Q. Lian, W. Wang, A. H. Milani, Z. Cui, N. T. Nguyen, M. Chen and L. A. Lyon, *ACS Macro Lett.*, 2017, **6**, 1245-1250.
10. J. P. S. Farinha, J. M. G. Martinho, A. Yekta and M. A. Winnik, *Macromolecules*, 1995, **28**, 6084-6088.
11. C. G. Wiener, C. Wang, Y. Liu, R. A. Weiss and B. D. Vogt, *Macromolecules*, 2017, **50**, 1672-1680.
12. R. Long, K. Mayumi, C. Creton, T. Narita and C.-Y. Hui, *Macromolecules*, 2014, **47**, 7243-7250.
13. D. C. Lin, J. F. Douglas and F. Horkay, *Soft Matter*, 2010, **6**, 3548-3561.
14. H. Zhang, H. Peng, Y. Li, Y. Xu and W. Weng, *Polymer*, 2015, **80**, 130-137.
15. J. Tian, T. A. Seery, D. L. Ho and R. Weiss, *Macromolecules*, 2004, **37**, 10001-10008.
16. J. Tian, T. A. Seery and R. Weiss, *Macromolecules*, 2004, **37**, 9994-10000.
17. J. Ilavsky, *J. Appl. Crystallogr.*, 2012, **45**, 324-328.
18. J. Tian, T. A. P. Seery, D. L. Ho and R. A. Weiss, *Macromolecules*, 2004, **37**, 10001-10008.
19. C. Wang, C. G. Wiener, Y. Yang, R. A. Weiss and B. D. Vogt, *J. Polym. Sci., Part B: Polym. Phys.*, 2017, **55**, 1036-1044.
20. S. Prevost, T. Lopian, M. Pleines, O. Diat and T. Zemb, *J. Appl. Crystallogr.*, 2016, **49**, 2063-2072.
21. S. Prevost, M. Gradzielski and T. Zemb, *Adv. Colloid Interface Sci.*, 2017, **247**, 374-396.
22. C. P. Cabry, L. D'Andrea, K. Shimizu, I. Grillo, P. Li, S. Rogers, D. W. Bruce, J. N. C. Lopes and J. M. Slattery, *Faraday Discuss.*, 2017, **206**, 265-289.
23. B. Hammouda, Probing Nanoscale Structures—The SANS Toolbox. http://www.ncnr.nist.gov/staff/hammouda/the_SANS_toolbox.pdf (accessed October 27, 2016).
24. M. Mihajlovic, M. Staropoli, M. S. Appavou, H. M. Wyss, W. Pyckhout-Hintzen and R. P. Sijbesma, *Macromolecules*, 2017, **50**, 3333-3346.
25. G. Beaucage, in *Polymer Science: A Comprehensive Reference*. K. Matyjaszewski and M. Möller, Elsevier, Amsterdam, 2012, Vol 2, pp. 399-409.

26. J. E. Mark and B. Erman, *Rubberlike elasticity: a molecular primer*, Cambridge University Press, 2007.
27. A. A. Gurtovenko and Y. Y. Gotlib, *J. Chem. Phys.*, 2001, **115**, 6785-6793.
28. S. A. Baeurle, A. Hotta and A. A. Gusev, *Polymer*, 2005, **46**, 4344-4354.
29. J. Hao and R. A. Weiss, *Macromolecules*, 2011, **44**, 9390-9398.
30. A. Gurtovenko and Y. Y. Gotlib, *J. Chem. Phys.*, 2001, **115**, 6785-6793.
31. H. Schiessel, R. Metzler, A. Blumen and T. Nonnenmacher, *J. Phys. A: Math. Gen.*, 1995, **28**, 6567.
32. D. Johnston, *Phys. Rev. B*, 2006, **74**, 184430.
33. T. L. Sun, T. Kurokawa, S. Kuroda, A. B. Ihsan, T. Akasaki, K. Sato, M. A. Haque, T. Nakajima and J. P. Gong, *Nat. Mater.*, 2013, **12**, 932.
34. H.-N. Lee, R. A. Riggleman, J. J. de Pablo and M. D. Ediger, *Macromolecules*, 2009, **42**, 4328-4336.
35. D. Chandler, *Nature*, 2005, **437**, 640.
36. M. Broniatowski and P. Dynarowicz-Łątka, *Journal of colloid and interface science*, 2006, **299**, 916-923.
37. V. H. Dalvi and P. J. Rossky, *Proceedings of the National Academy of Sciences*, 2010, **107**, 13603-13607.
38. Q. Chen, C. Huang, R. A. Weiss and R. H. Colby, *Macromolecules*, 2015, **48**, 1221-1230.



Strain rate dependent nanostructure evolution of physical hydrogels were probed by *in-situ* SAXS and correlated with mechanical responses of hydrogels.